ISSN 0001-4338, Izvestiya, Atmospheric and Oceanic Physics, 2012, Vol. 48, No. 2, pp. 152–168. © Pleiades Publishing, Ltd., 2012.
Original Russian Text © Ph.L. Bykov, V.A. Gordin, 2012, published in Izvestiya AN. Fizika Atmosfery i Okeana, 2012, Vol. 48, No. 2, pp. 172–188.

Objective Analysis of the Structure of Three-Dimensional Atmospheric Fronts

Ph. L. Bykov[a, b, c] and V. A. Gordin[b, c]

[a] *Moscow State University, Moscow, 119992 Russia*
[b] *Hydrometeorological Centre of Russia, Bol'shoi Predtechenskii per. 9–13, Moscow, 123376 Russia*
[c] *National Research University—Higher School of Economics, Myasnitskaya ul. 20, Moscow, 101000 Russia*
e-mail: vagordin@mail.ru

Received October 15, 2010

Abstract—A computational method for diagnosing three-dimensional atmospheric fronts from temperature, wind, and geopotential fields on a three-dimensional regular grid is proposed. The criterion, which serves for the diagnosis of atmospheric fronts, is discussed. The weights of the input information about the mentioned fields are optimized based on the maximal difference between the correlation functions for (a) pairs of particles separated by the front and (b) pairs from one synoptic mass. These weights were different for different baric levels. The correlation functions and the optimization of weights were estimated on the basis of the archive of fields of the NCEP objective analysis on the half-degree latitude–longitude grid and data from aerological observations. The results of numerical experiments on the construction of atmospheric fronts are presented. Applying the described method to fields predicted for a term of up to 36 h showed that errors in the prognostic models introduce a relatively weak distortion into the geometry of atmospheric fronts.

Keywords: contact discontinuity, predictor, Hessian, correlation function, compact scheme, wind, geopotential, temperature.

DOI: 10.1134/S0001433812020053

INTRODUCTION

The evolution of the atmosphere could be described by the system of gas dynamics equations supplemented by nonadiabatic terms, which correspond to turbulent viscosity, solar radiation, phase transitions, etc. The discontinuities in solutions of the ideal system (i.e. without additional terms) could be classified as shock-wave discontinuities and tangencial discontinuities of the solutions of the quasi-linear system of partial differential equations.

Shock waves can be natural or anthropogenic and they propagate at the speed of sound. Long (on the order of thousands of kilometers) tangential discontinuities are interpreted as atmospheric fronts.

In the wind field (on the atmospheric front line), the wind component tangential to this line is discontinuous, whereas the perpendicular wind component is continuous but has a kink. In the real world, the atmospheric front clearly visible in one of the fields might be negligible in the other. All available information about meteorological fields must be used for practical numerical analysis of the front geometry.

This work is dedicated to the diagnostics of atmospheric fronts on the basis of objective analysis of wind, geopotential, and temperature on a regular three-dimensional grid in a p coordinate system. Our method is also applicable to analogous prognostic fields.

In the ideal three-dimensional model [1], the atmospheric front is a surface in a three-dimensional space inclined with respect to the sea level. A typical inclination angle is ~1°.

For the ideal system, it is possible to prove instability of tangential discontinuities with respect to small disturbances [2]. However, for a viscous model taking into account the vertical stratification of the atmosphere, tangential discontinuities can exist for a finite time, which is supported by meteorological observations. When the model includes turbulent viscosity, the two dimensional surface is replaced by the atmospheric front that is about tens of kilometers wide and sometimes moves with time. The atmospheric fronts that are less than one kilometer are very rare.

We shall look for the atmospheric front in the form of the intersection with one of the following surfaces: the baric surface $p = \text{const}$, a level in a σ coordinate system, the Earth, and the real or imaginary sea level. Our initial data come either from observations (at a discrete set of stations) or from a regular prognostic grid.

In a three-dimensional objective analysis, it is also necessary to establish the relation between frontal lines at adjacent baric levels and to construct an inclined surface in the three-dimensional space, i.e., the atmospheric front. In this case the surface we are looking for

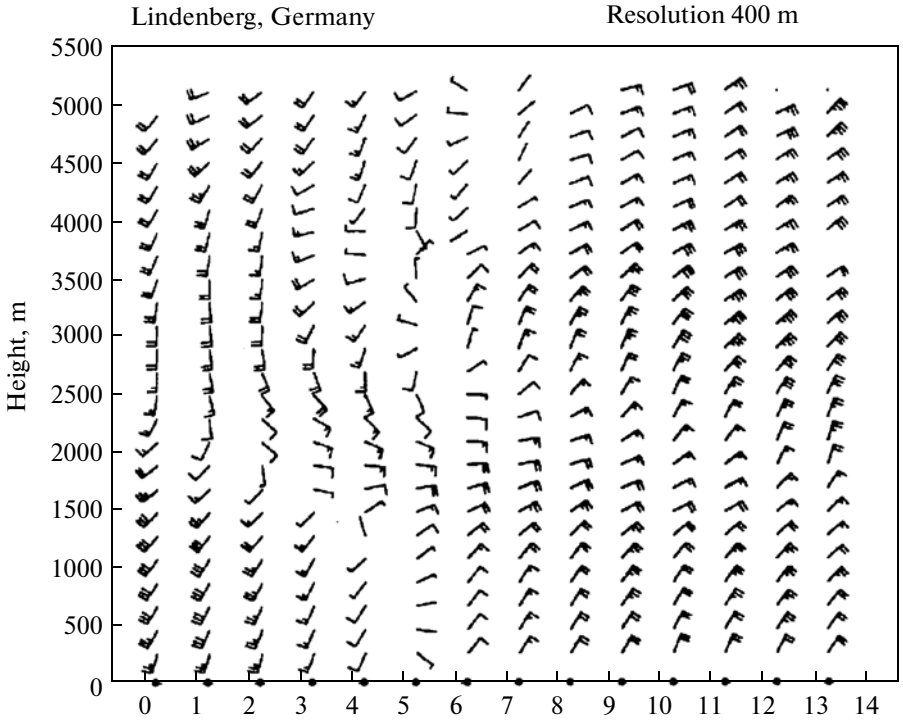

Fig. 1. (From [6]). Horizontal wind field (designation by arrows) measured with a profiler during the atmospheric front passage over the Lindenberg station (Germany) in the variables t (h) and z (m). The long feather on the arrow corresponds to 5 m/s, and the short one corresponds to 2.5 m/s.

may not necessarily be smooth; it may have specific features, holes, etc.

The figure 1 shows an example of the wind field that is changing from the South-West one to the North-West one. At each height, the time of the change in direction to the opposite one took 1–2 h, even if the wind velocity component normal to the front was very small. The temporal vertical geometry of the changes presented in Fig. 1 is rather complex and, consequently, it is impossible to assume that the frontal surface is well approximated globally by a moving inclined plane. On the other hand, the results of measurements at the neighboring levels are rather close to each other here. Consequently, approximately the same density of vertical levels is required for an adequate description of the atmospheric front geometry.

The following definitions for the free atmosphere are proposed in [3]: the baroclinic zone (whose usual width is 200–800 km), if $|\nabla T| > 1°\text{C}/100$ km, and the frontal zone (50–200 km), if $|\nabla T| > 3°\text{C}/100$ km. Our criteria for the atmospheric front are more complex but give better results.

To describe the front geometry properly, we should find the definition of the front that suits computational methods best. In our opinion, the adequacy of the separation of synoptic air masses by the drawn fronts can be taken as the optimality criterion. In other words, the criterion of the front should satisfy the following condition: the difference between the values of correlation function for the meteorological fields in the case when two points are separated by the front line and are not separated by the front line should be the largest possible.

1. ESTIMATING DERIVATIVES OF METEOROLOGICAL FIELDS AND CONSTRUCTING THE FIELDS OF PREDICTORS OF THE ATMOSPHERIC FRONT

In this section of both main meteorological fields we shall construct a predictor field. This will be a scalar field, whose larger values correspond to bigger probability to find the atmospheric somewhere nearby. We emphasize that the term "predictor" field has no connection to "prediction" here.

1.1. Atmospheric Front and Pressure Field

It is known (see, for example, [4, 5]) that the atmospheric front manifests itself in the pressure field p_s as "a hidden hollow." According to the classical approach, the Laplacian Δp_s is estimated based on grid values. At the front line, this parameter takes large values.

For the hollow, the second derivative is large (compared with second derivatives at points not located on

the front) only in the direction perpendicular to the front line. The Laplacian is the sum of the second derivatives of p_s in two orthogonal directions, for example, along and across the front. The second derivative of p_s along the front is bounded, and, if it is assumed to be statistically independent of the second derivative in the orthogonal direction, the addition of this derivative to the hollow predictor will deteriorate its quality, on average, $\sqrt{2}$ times.

To get rid of the second derivative along the front line, we use a different functional indicator, i.e., the largest eigenvalue $L(x, y)$ of the Hessian, which for a plane and a sphere takes the forms

$$H(x,y) = \begin{Vmatrix} \frac{\partial^2 p_s}{\partial x^2} & \frac{\partial^2 p_s}{\partial x \partial y} \\ \frac{\partial^2 p_s}{\partial y \partial x} & \frac{\partial^2 p_s}{\partial y^2} \end{Vmatrix} \text{ and}$$

$$H(\lambda,\varphi) \qquad (1)$$

$$= \begin{Vmatrix} \frac{1}{\sin\varphi}\left(\cos\varphi\frac{\partial p_s}{\partial\varphi} + \frac{1}{\sin\varphi}\frac{\partial^2 p_s}{\partial\lambda^2}\right) & \frac{\partial}{\partial\varphi}\left(\frac{1}{\sin\varphi}\frac{\partial p_s}{\partial\lambda}\right) \\ \frac{\partial}{\partial\varphi}\left(\frac{1}{\sin\varphi}\frac{\partial p_s}{\partial\lambda}\right) & \frac{\partial^2 p_s}{\partial\varphi^2} \end{Vmatrix}$$

respectively.

To calculate the function $L(x, y)$, it is necessary to estimate all second derivatives. We estimate them using special discrete Fourier transform (see paragraph 1.4) and compact schemes [7] on the sphere and on the plane, respectively.

1.2. Discrete Fourier Transform for Functions on a Two-Dimensional Sphere and Calculation of Their Derivatives

Let A_n be the Euclidean space of functions on a regular n-polygon. The functions $\{\exp ijx\}_{j=0}^{n-1}$ form an orthogonal basis in this space. The Fourier transform of the function $f(x) \in A_n$ is a set of function's coefficients $f(x)$ with respect to the basis $\tilde{f}(j) = F_{x\to j}[f(x)]$:

$$\tilde{f}(j) = \frac{1}{n}\sum_{k=1}^{n} f(x_k)e^{-ix_k j}, \quad j = 0,\ldots,n-1.$$

Similarly, the inverse Fourier transform (prototype) is $f(x_k) = F_{j\to x}^{-1}\left[\tilde{f}(j)\right]$:

$$f(x_k) = \frac{1}{2\pi n}\sum_{j=0}^{n-1} \tilde{f}(j)e^{ix_k j}, \quad k = 1,\ldots,n.$$

If f takes only real values, for any number $1 \le j < n$, the values of $\tilde{f}(j)$ and $\tilde{f}(n+1-j)$ are conjugated to each other.

The image of the Fourier transform of the derivative $\frac{\partial^s}{\partial x^s} f(x)$ at $f \in A_n$ is equal to $(ij)^s \tilde{f}(j)$. Therefore,

$$\frac{\partial^s}{\partial x^s} f(x) = F_{j\to x}^{-1}\left[(ij)^s F_{x\to j}(f(x))\right]. \qquad (2)$$

Now we can calculate the derivative with respect to the longitude of any order from a function discretely specified on a sphere.

For meteorological problems on the globe, the Fourier transformation in terms of longitude is natural and useful. However, as the pole is approached, the grid step decreases many times; therefore, the closer one gets to the pole, the larger the number of longitudinal modes must be nullified (because modes with large numbers are mostly due to errors in discretization during the transmission through communication channels). We did not nullify modes with indices smaller than $m = 2 + m_{\max}(n-1)\sin\varphi$, where φ is the colatitude, $m_{\max} = 1/2$ in the temperature gradient calculation, and $m_{\max} = 1/4$ in other cases. For smoothing the results, after the differentiation, the jth mode was additionally multiplied by $\cos\frac{\pi(j-1)}{2m}$.

1.3. Calculation of Derivatives with Respect to Longitude using the Fourier Transform

Let us consider a smooth scalar function on a sphere $P(\lambda, \varphi)$ and the result of its Fourier transformation with respect to longitude $f_j(\varphi) = F_{\lambda\to j}[P(\lambda,\varphi)]$. The asymptotics at the pole (i.e., at $\varphi \to 0$) for the jth mode takes the form (see [8–10]):

$$f_j(\varphi) = \gamma_0\varphi^j + \gamma_1\varphi^{j+2} + \gamma_2\varphi^{j+4} + \ldots \qquad (3)$$

With respect to the pole point, the odd mode behaves as an odd function; i.e., the function

$$\hat{f}_j(\varphi) = \begin{cases} f(\varphi) & \varphi \in [0;\pi], \\ -f(-\varphi) & \varphi \in [-\pi;0] \end{cases}$$

is smooth at the poles ($\varphi = 0$, π) and it can be considered as a smooth function on a circle $\varphi \in [-\pi;\pi]$. The even mode is an even function with respect to the pole points and, consequently, the function

$$\hat{f}_j(\varphi) = \begin{cases} f(\varphi) & \varphi \in [0;\pi], \\ f(-\varphi) & \varphi \in [-\pi;0] \end{cases}$$

is smooth at the points $\varphi = 0$, π and it can also be considered as a smooth function on a circle.

We shall differentiate the function $\hat{f}_j(\varphi)$ of latitude using Fourier transform and formula (2) in particular. The restriction of the result onto the interval $[0;\pi]$, will give us the derivative $f_j'(\varphi)$ at $\varphi \in [0;\pi]$.

However, if we replace the scalar function by the one of the components of the vector field, the asymptotics for the jth mode in the pole vicinity will be [10]:

$$f(\varphi) = \begin{cases} \gamma_1\varphi^{j-1} + \gamma_2\varphi^{j+1} + \gamma_3\varphi^{j+3} + \ldots, & j > 0 \\ \gamma_1\varphi + \gamma_2\varphi^3 + \gamma_3\varphi^5 + \ldots, & j = 0. \end{cases} \quad (4)$$

This makes it possible to use the same algorithm of the vector field components for calculating derivatives as was used for scalar functions by interchanging the cases of even and odd modes. The boundary conditions and asymptotics for vector fields in the pole vicinity are considered more comprehensively in [8].

1.4. More Efficient Method for Calculating the Derivative with Respect to Latitude

Now, we present a method for calculating the derivative with respect to latitude, which does not require the calculation of the forward and inverse Fourier transforms in terms of longitude and, consequently, is faster than the method described in Section 1.3.

In the case of differentiating a scalar function with respect to latitude, we consider this function on the meridian given, which is supplemented to a periodic function by the values on the opposite meridian:

$$\hat{f}(\lambda,\varphi) = \begin{cases} f(\lambda,\varphi), & \varphi \in [0,\pi], \ \lambda \in [0,2\pi), \\ f(\lambda+\pi,-\varphi), & \varphi \in [-\pi,0], \ \lambda \in [0,\pi], \\ f(\lambda-\pi,-\varphi), & \varphi \in [-\pi,0], \ \lambda \in [\pi,2\pi). \end{cases} \quad (5)$$

In the case of the vector field components, this function is supplemented by the opposite values:

$$\hat{f}(\lambda,\varphi) = \begin{cases} f(\lambda,\varphi), & \varphi \in [0,\pi], \ \lambda \in [0,2\pi), \\ -f(\lambda+\pi,-\varphi), & \varphi \in [-\pi,0], \ \lambda \in [0,\pi], \\ -f(\lambda-\pi,-\varphi), & \varphi \in [-\pi,0], \ \lambda \in [\pi,2\pi). \end{cases} \quad (6)$$

The negative sign appears in (6) due to the fact that, during the transition through the pole, the positive directions of the zonal and meridional wind components in spherical coordinates become negative.

On the latitude–longitude grids, which are used at present in analytical and prognostic operational schemes, the number of points in longitude is even and the grid function values on the meridian opposite to the given meridian are also known. The continuations of functions (5) and (6) are induced by the sphere mapping onto a tore on which all values of the initial function are repeated twice. For passing back to the sphere, it is sufficient to restrict the function by positive values of φ.

1.5. Extrapolation to Pole Points

Many formulas given below contain the operation of division by sinφ, which is uncertain at the pole points. However, in all these formulas, the numerator at the pole point is also zero. In order to accomplish the division at the pole point, we first perform it at all other points, whereupon we extrapolate[1] the result along the colatitude into the pole points, using asymptotics (3) and (4).

Let us construct formulas of the fifth order of accuracy for the extrapolation of the smooth scalar function into the North Pole point. All modes with nonzero indices in longitude, $j \neq 0$, are zero at the pole points. Rewrite formula (3) for $j = 0$:

$$f_0(\varphi) = \gamma_0 + \gamma_1\varphi^2 + \gamma_2\varphi^4 + O(\varphi^6).$$

The values corresponding to the zero mode $y_1 = f_0(h)$, $y_2 = f_0(2h)$, $y_3 = f_0(3h)$, are assumed to be known. We obtain the system of linear equations for γ_0, γ_1, and γ_2:

$$\begin{cases} y_1 = \gamma_0 + h^2\gamma_1 + h^4\gamma_2, \\ y_2 = \gamma_0 + 4h^2\gamma_1 + 16h^4\gamma_2, \\ y_3 = \gamma_0 + 9h^2\gamma_1 + 81h^4\gamma_2, \end{cases}$$

from which we find that $f_0(0) = \gamma_0 = (15y_1 - 6y_2 + y_3)/10$.

The formula for extrapolating the vector field component differs from the formula for the scalar function only by the fact that, instead of $j = 0$, the modes with $j = 1$ and $n - 1$ are nonzero at the pole point.

1.6. Hesse Matrix in Spherical Coordinates

Suppose that we know the values of a certain real function $P(\lambda_k, \varphi_n)$, $0 \le p \le n$, $0 \le k \le m$, where φ is the latitude and λ is the longitude, at the vertices of the latitude–longitude grid.

Let us find the expression for the Hesse matrix at the point of the sphere with the coordinates (λ^0, φ^0) for a function in spherical coordinates. In local geodetic coordinates x and y, where y corresponds to the colatitude and x corresponds to the longitude, this expression coincides with expression (1) for the tangent Cartesian plane at $x = y = 0$.

The differentiation with respect to y yields the same result as the differentiation with respect to φ, because $y = \varphi - \varphi^0$ and, consequently, the geodetic coordinate $x = 0$ coincides with the curve $\lambda = \lambda^0$.

The geodetic coordinate $y = 0$ touches upon the parallel $\varphi = \varphi^0$ (Fig. 2); therefore, the first derivative

[1] This is actually not an extrapolation but interpolation, because the points located near the pole completely surround it.

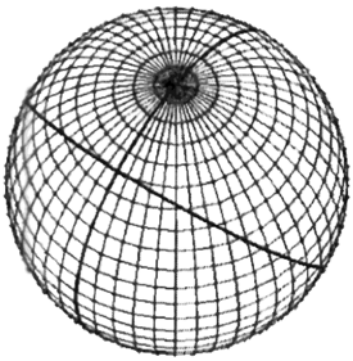

Fig. 2. Latitude–longitude grid and geodetic lines on a sphere.

with respect to longitude coincides with the first derivative with respect to x divided by $\sin\varphi^0$:

$$\frac{\partial P}{\partial x}(\lambda^0,\varphi^0) = \frac{1}{\sin\varphi^0}\frac{\partial P}{\partial \lambda}(\lambda^0,\varphi^0).$$

Let us find the second derivative of the function P with in terms of x. We rewrite the equation for the geodetic coordinate $y = 0$ in spherical coordinates:

$$\varphi = \arctan\left(\frac{\tan\varphi^0}{\cos(\lambda-\lambda^0)}\right).$$

Twice differentiating the λ-function

$$P\left(\lambda, \arctan\left(\frac{\tan\varphi^0}{\cos(\lambda-\lambda^0)}\right)\right),$$

with respect to λ and dividing it by $\sin^2\varphi^0$, we obtain

$$\frac{\partial^2 P}{\partial x^2} = \frac{1}{\sin\varphi^0}\left(\cos\varphi^0\frac{\partial P}{\partial\varphi} + \frac{1}{\sin\varphi^0}\frac{\partial^2 P}{\partial\lambda^2}\right).$$

Thus, the Hesse matrix for a smooth function in spherical coordinates has form (1), and, after the Fourier transformation in terms of longitude $F_{\lambda\to j}$:

$$\tilde H(j,\varphi) = \begin{Vmatrix} \frac{1}{\sin\varphi}\left(\cos\varphi\frac{\partial\tilde P}{\partial\varphi} - \frac{j^2\tilde P}{\sin\varphi}\right) & \frac{\partial}{\partial\varphi}\left(\frac{ij\tilde P}{\sin\varphi}\right) \\ \frac{\partial}{\partial\varphi}\left(\frac{ij\tilde P}{\sin\varphi}\right) & \frac{\partial^2\tilde P}{\partial\varphi^2} \end{Vmatrix}.$$

Note that the difference of the functions $\cos\varphi\frac{\partial\tilde P}{\partial\varphi}$ and $\frac{j^2\tilde P}{\sin\varphi}$ vanishes at the pole point; however, speaking generally, not all of them vanish separately at $j \neq 0$.

Now, to estimate the largest eigenvalue of the Hesse matrix for the function specified on the latitude–longitude grid, it is necessary to approximate the first and second derivatives with respect to φ of the functions $\tilde P$ and $\frac{ij\tilde P}{\sin\varphi}$, perform the inverse Fourier transforms in terms of longitude, and solve the problem of finding the eigenvalues for the second-order matrix at all points of the sphere.

1.7. Atmospheric Front in the Wind Field

Intersections of the wind field with the front surface can be also detected from the wind field at a specified baric level $p = \text{const}$, because the tangential (to the front surface) component of the wind (which can be "blurred" under the action of turbulent viscosity) is discontinuous here.

To find the atmospheric front zone at a baric level, we calculate the vertical component of the wind velocity vortex, i.e., the scalar function of u and v, where u and v, are the wind components corresponding to y and x in Cartesian coordinates, respectively:

$$\zeta = \frac{\partial u}{\partial y} - \frac{\partial v}{\partial x}.$$

The vortex in spherical coordinates (u is the zonal component of the wind, and v is its meridional component)

$$\zeta = \frac{1}{\sin\varphi}\left(\frac{\partial(u\sin\varphi)}{\partial\varphi} - \frac{\partial v}{\partial\lambda}\right).$$

The wind component tangential to the front line can undergo a discontinuity; however, the orientation of the discontinuity line is unknown beforehand.

Now, we introduce a unit vector perpendicular to the discontinuity line $\mathbf{b} = \langle\cos s, \sin s\rangle$, and denote the wind projection $\langle u, v\rangle$ on $\mathbf{b}$ as w. We try to determine R, i.e., the maximal (with respect to s) value of the derivative of w in the direction $\mathbf{b}^\perp = \langle -\sin s, \cos s\rangle$, which is perpendicular to $\mathbf{b}$. On the tangential discontinuity, R is infinite. The velocity vortex will be obtained if the derivative of the wind projection on $\mathbf{b}$ along $\mathbf{b}$ is added to R. This second term on the front line is a bounded function even in an ideal model, and its addition in approximate calculations only noises the result. The direct calculation proves the following lemma.

Table 1. RMS values of predictors

Level, hPa	RMS value of $\|\nabla T\|$, 10^{-4} °C/km	RMS value of $\|L\|$, 10^{-8} km^{-1}	RMS value of $\|R\|$, 10^{-6} s^{-1}	Level, hPa	RMS value of $\|\nabla T\|$, 10^{-4} °C/km	RMS value of $\|L\|$, 10^{-8} km^{-1}	RMS value of $\|R\|$, 10^{-6} s^{-1}
1000	175 (264)	50 (90)	19.3 (20.3)	200	98.9	34.1	34.2
925	135 (158)	45.1 (72.4)	27.4 (28.2)	150	77.9	26.8	25.3
850	130 (148)	41.6 (57.4)	27.2 (28.2)	100	77.7	23.6	20
700	128 (138)	35.3 (37)	28 (28.7)	70	73.3	23.3	20.3
500	101	42.4	35.1	50	67.6	25.3	22.4
400	93.8	53.1	42.4	30	67.2	31.3	27.7
300	86.4	55	48.1	20	73.1	36.4	32.6
250	99.7	46.1	43.8	10	79.7	47.1	39.8

Note: Averaging over 250 days from March to November 2007, inclusively, using the data of the 12-h NCEP forecast by 00:00 GMT on the grid with a step of 1°. The values obtained from the averaging over the entire grid rather than only over the points located above the earth's surface are indicated in parentheses.

Lemma 1. The value R is equal to the largest eigenvalue of the matrix:

$$K = \frac{1}{\sin\varphi}\begin{Vmatrix} \dfrac{\partial(u\sin\varphi)}{\partial\varphi} & \dfrac{1}{2}\left(\dfrac{\partial(v\sin\varphi)}{\partial\varphi} - \dfrac{\partial u}{\partial\lambda}\right) \\ \dfrac{1}{2}\left(\dfrac{\partial(v\sin\varphi)}{\partial\varphi} - \dfrac{\partial u}{\partial\lambda}\right) & -\dfrac{\partial v}{\partial\lambda} \end{Vmatrix} \text{ or}$$

$$K = \begin{Vmatrix} \dfrac{\partial u}{\partial y} & \dfrac{1}{2}\left(\dfrac{\partial v}{\partial y} - \dfrac{\partial u}{\partial x}\right) \\ \dfrac{1}{2}\left(\dfrac{\partial v}{\partial y} - \dfrac{\partial u}{\partial x}\right) & -\dfrac{\partial v}{\partial x} \end{Vmatrix}$$

in the spherical and planar cases, respectively.

Remark 1. If the wind is geostrophic [5, 9], Hesse matrix (1) for the geopotential coincides with the matrix $K(\varphi, \lambda)$. In this case, any of the terms $\dfrac{\partial(v\sin\varphi)}{\partial\varphi}$ and $-\dfrac{\partial u}{\partial\lambda}$ can be taken as extradiagonal elements.

Remark 2. The wind component normal to the front may have a kink on the front line; however, this fact cannot be used for the front diagnostics in a numerical analysis. Indeed, inaccuracies in the front direction calculation lead to the fact that the calculated wind field component normal to the front will not coincide with the true component and will not necessarily be continuous. The subsequent calculation of the second derivative will yield an incorrect result.

1.8. Atmospheric Front in the Temperature Field

In the temperature field at a fixed baric level, the atmospheric front in an ideal model will represent a jump line of a two-dimensional function. In order to diagnose the atmospheric front from temperature data at a certain baric level, the absolute value of the horizontal temperature gradient $|\nabla T|$, is calculated according to our algorithm, although other variants are possible [11].

2. CONSTRUCTION OF FRONTAL ZONES

Three fields of the front predictors were constructed on the basis of the main meteorological fields (geopotential, wind, and temperature) on the latitude–longitude grid with the step h (the curvature of the geopotential plot $L(\varphi, \lambda)$, the largest eigenvalue $R(\varphi, \lambda)$ of the matrix $K(\varphi, \lambda)$, and the temperature gradient magnitude, respectively). These fields take comparatively large values near the front. Now, we construct frontal zones on the basis of these predictor fields (or their combinations) and compare the results.

2.1. Normalization of Predictor Fields

First, we normalize the predictor fields, having divided them by the mean values, to exclude the dependence of the used algorithm and constants on neither the baric level nor the considered predictor field. In this case, we can use various combined predictors, for example, the mean arithmetic of some two initial predictors.

We normalize each field, having divided it by its RMS value (see Table 1) taken from the values only at the grid points located over the earth's surface. Without this stipulation (about taking the parenthetical values in Table 1), we risk obtaining only fictitious frontal

zones coinciding with mountain massifs at low baric levels (700 hPa and below).

Indeed, Table 1, together with the RMS values, gives the values (substantially larger for $|\nabla T|$ and $|L|$) averaged over the entire grid in parentheses and not only over the points located above the earth's surface.

Below, we use the predictors normalized in accordance with Table 1 everywhere.

2.2. Construction of Frontal Zones at Baric Levels

Now, we briefly describe the algorithm for the construction of frontal zones, which obtains a discrete field P at the input, i.e., a certain normalized predictor of the atmospheric front, and yields a set consisting of squares with sides equal to the grid step and centers coinciding with grid points at the output.[2] All sets constructed below consist of such squares; therefore, we identify these squares and their centers.

The grid point $\mathbf{x}_*$ is called "suspicious" in belonging to the frontal zone if $P(\mathbf{x}_*) > C_0$ (it was assumed that $C_0 = 0.6$).

Suppose that $A(P)$ is a set of squares with sides equal to h and centers at "suspicious" points of the grid. In this case, $A(P)$ a fortiori contains all frontal zones; however, it can be too thick (i.e., "includes extra" points).

The main computational problem is to identify among a set of close suspicious points the points near which the front is most clearly pronounced. The chosen points must form a certain line, which will be called the frontal line.

Let us formalize the notion of the ridge (the ridge in the predictor field will be interpreted as the atmospheric front). The ridge for the two-dimensional field P is the line whose points are characterized in the following way: the function P along the straight lines close to its normal has a conditional local maximum precisely at the ridge point. We call such straight lines good for the given point of the ridge. If the ridge is a thin (in the scale h) band, then at each point good straight lines cover a fairly wide spectrum.

The ridge we were looking for $B(P)$ is a subset of the discrete set $A(P)$. Without additional interpolation, we can use on the grid not a continuum of straight lines passing through the grid point $\mathbf{x}_* \in A(P)$, but only four straight lines (two lines parallel to the axes and two lines intersecting them at an angle of 45°) connecting this grid point with two out of eight neighboring points. We propose the following condition for "two neighboring straight lines" (the TNL condition). Let us consider two pairs of straight lines passing through the point $\mathbf{x}_*$. The first pair includes straight lines parallel to the coordinate axes; the second pair includes straight lines located at an angle of 45° to the coordinate axes. The square K (where $\mathbf{x}_*$ is the center of the square K from $A(P)$) will be included into $B(P)$ only if at least one straight line from each pair is good for the point $\mathbf{x}_*$. An equivalent formulation is as follows: among four straight lines, we can identify two good straight lines and the angle between them will be 45°.

Under the TNL condition, the set $B(P)$ is not too thick, which is stated by the following lemma.

Lemma 2. If for each point of the set $B(P)$, either the horizontal or the vertical straight line passing through it is good, then $B(P)$ will contain none of the four points of the grid $A_1A_2A_3A_4$ which are forming the square with the side h.

One can see from the Fig. 3 that this algorithm may give too many connected components of the set $B(P)$ and the final result will contradict to the expected one. Let us join some connected components together via returning certain points from $A(P)$ back to $B(P)$. In other words, we construct the set $C(P)$ consisting of points belonging to $B(P)$ and squares from $A(P)$, which are simultaneously neighboring two different connectivity components of $B(P)$ (we assume that each square of the grid has eight neighboring squares). However, as Fig. 3 shows, we have added an excessive number of squares into $C(P)$. Therefore, the algorithm must be refined by adding only the squares for whose centers at least one of four straight lines is good.

Further, to suppress possible noises, we eliminate from $C(P)$ connected components whose area (note that the area of the grid square at the colatitude φ is $2h\sin(h/2)\sin\varphi \approx h^2\sin\varphi$) is smaller than $5h^2$ or connected components where maximal value of the field P is smaller than a certain constant C_1 (for example, $C_1 = 1$).[3] Otherwise, the front is regarded as too short or weakly pronounced, respectively (Fig. 4).

We shall refer to the set $C(P)$ as "the set of possible frontal zones."

2.3. Vertical Correlation of Frontal Zones

To construct frontal zones we have used the fields of objective analysis (OA) field and forecasts for 12, 24, and 36 h with the vertical resolution 50 hPa and the horizontal resolution 0.5° × 0.5°. Therefore, in the three-dimensional problem, in passing by one level downward, the horizontal displacement of a real frontal zone cannot exceed 1–2 grid steps along the horizontal (otherwise we deal with different frontal zones). In our experiments, the highest quality frontal zones were constructed at levels of 400–300 hPa; the lower

[2] A detailed description of the algorithm is rather cumbersome and will be presented in a separate publication.

[3] These noises can be caused, for example, by the criterion instability: at a small disturbance of the field P, a square previously included into $B(P)$ can be rejected.

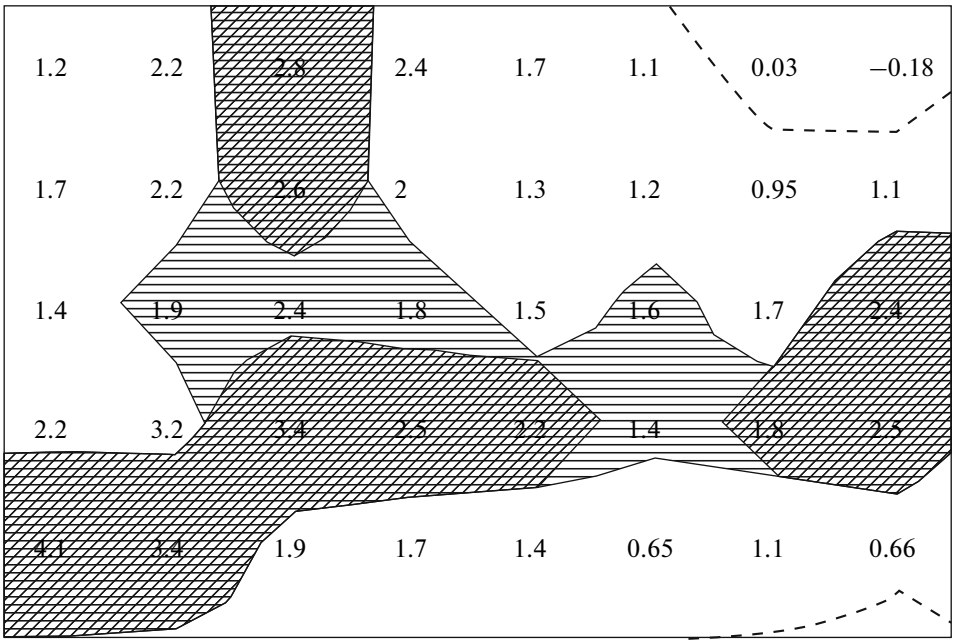

Fig. 3. Real example of the operation of the algorithm for the identification of frontal zones. The dotted line outlines the set of "suspicious" points $A(P) = \{\mathbf{x} | P(\mathbf{x}) > C_0 = 0.6\}$. The diagonal dashed line outlines the set $B(P)$, and the horizontal dashed line outlines the set of constructed frontal zones $C(P)$. In the figure, the boundaries of these zones are smoothed; the sets $A(P)$, $B(P)$, and $C(P)$ consist of squares with sides parallel to the axes. The values of the field L are plotted. If only the points for which a good straight line exists are added to $C(P)$, in the set $C(P)\backslash B(P)$ there will be no squares with values of 1.4, 1.8, and 1.9 in the centers (only the values 1.6 and 2.4 will remain).

the level is, the worse the quality of construction is, i.e., some front sites are pronounced less clearly and the front becomes discontinued. An example of the vertical meridional section with the drawn fronts is presented in Fig. 5.

On the contrary, frontal zones near the earth's surface and at small heights are synoptically most interesting. During the successive (from top to bottom) construction of frontal zones, at each new baric level, we take into account the result of an analysis of the construction at the previous level. The level 400 hPa will be assumed as basic, and, at this level, the constant $B_v = 0.2$ will be added to the predictor field. Each time, passing to the construction of frontal zones at lower levels, we add the constant "bonus" B_v. to the predictor field near the front zone at a higher level (directly over the front points at the higher level, as well as at a distance of no more than three steps along the horizontal toward the temperature gradient, i.e., 1.5° of latitude or longitude). At such a vertical connection, frontal zones will be more continuous along the vertical and, since the bonus is constant, there will be no displacements of frontal zones caused by the bonus (the maximum is attained at the same ridge as without the bonus).

3. CALCULATION OF CORRELATION FUNCTIONS

The distinction between the air masses separated by the constructed frontal regions is the main quality criterion of the algorithm used for the construction. Assuming the hypothesis of homogeneity and isotropy of meteorological fields inside the air mass, we estimate from horizontal variables [7, 12–14] two-dimensional auto- and cross-correlation functions (CFs) of the temperature, geopotential, and longitudinal and transverse wind components at different baric levels from the distance along the horizontal. Three-dimensional CFs were estimated in [12, 13]; however, we thought that the calculation of two-dimensional CFs was sufficient for the purposes of this article.

The anisotropy was estimated in [7, 13], and it was shown that the isotropy hypothesis has the largest error in the tropical stratosphere. In the region of interest to us (extratropical troposphere), this hypothesis is adequate for observations.

3.1. Determination of the Belonging of Two Points at One Level to Different Air Masses

Suppose that the two points W and Q are given at one baric level, and it is necessary to determine whether the front passes between them, i.e., whether these points belong to the same air mass or to different

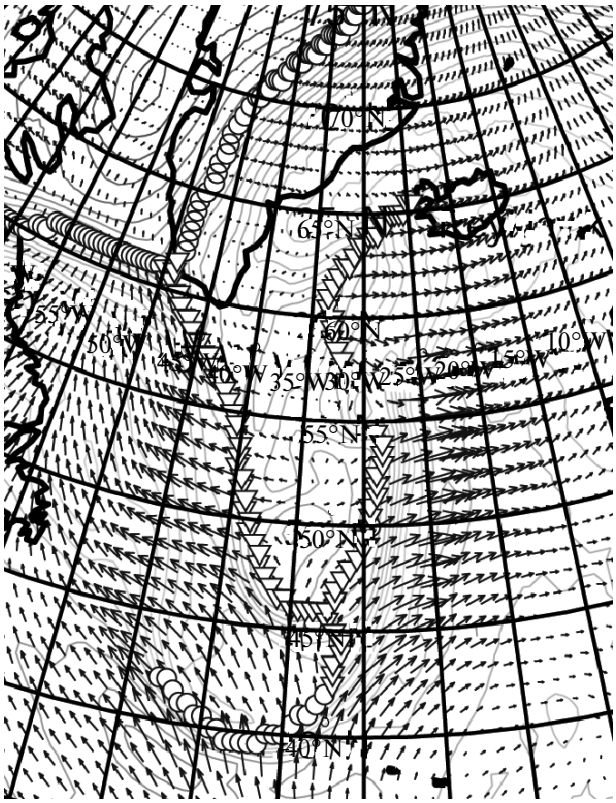

Fig. 4. Atmospheric front lines over the North Atlantic at the level 500 hPa calculated using the optimal criterion (see Section 4) from the OA NCEP data for 00:00, April 10, 2010. The temperature contours and the wind field are shown. Part of the front is well pronounced in the temperature field (circles on the line show this) and part of the front is well pronounced in the geopotential field (triangles).

air masses. If $W \in C(P)$ or $Q \in C(P)$, it is impossible to decide which of two possibilities takes place and, therefore, in the calculation of CFs (see below), such pairs of stations were rejected in the statistics.

If it is possible to find a way from W to Q, close to the shortest distance between them and not crossing frontal regions, we assume that W and Q lie in one air mass (case A); otherwise they belong to different air masses (case B).

Let us connect W and Q by the shortest geodetic line and consider its h vicinity U_h. If both of the initial points lie in one connectivity component (here, we assume that each square has four neighboring squares) of the set $U_h \backslash C(P)$, we shall assume that they belong to one air mass; otherwise they belong to different air masses.

The algorithm used can be substantially faster if successive sections by meridians rather than the set $U_h \backslash C(P)$ are considered.

3.2. Normalization of Meteorological Fields

To calculate the CFs of the main meteorological fields, first it is necessary to normalize them, i.e., subtract the mean $Sf(\mathbf{x})$ and divide by the root from the estimate of variance:

$$F(\mathbf{x}) = \frac{f(\mathbf{x}) - Sf(\mathbf{x})}{\sqrt{S(f(\mathbf{x}) - Sf(\mathbf{x}))^2}}.$$

The following estimations of the mean value $Sf(\mathbf{x})$ are possible.

(1) Monthly mean (or decadal mean) value.

(2) ~~Prediction~~ by the moment that $f(\mathbf{x})$ is achieved with the minimal term of forecast (as a rule, 6 or 12 h).

(3) Sum of the minimal-term forecast and the mean deviation of the fact from the ~~prediction~~ for a given station.[4]

The first case is more important for understanding the atmospheric physics, whereas the second and third cases are more important for the practical task of analysis and ~~prediction~~.[5] If in the second case the CFs for points separated by the constructed frontal zones differ noticeably from the CFs for points not separated by such zones, then, by using in either case its own CF instead of the averaged CF, we can decrease the error of interpolation into grid points and improve the OA fields (and, consequently, the forecast based on them), especially near frontal zones.

In this work, we used the simplest method of normalization (see item (1)). The fields from our archive containing 336 fields of the NCEP analysis on the grid with the step 0.5° × 0.5° were used as fields for the construction of predictors.

3.3. Estimation of Correlation Functions

For estimating two-dimensional CFs (depending on the distance and level), we unite various pairs of stations into groups based on the distance between them: the first group from 0 to $\Delta r = 50$ km, the second group from Δr to $2\Delta r$, etc. We do not consider the stations with the distance r between them exceeding $R =$ 3000 km or the pairs of stations in which at least one station is located south of 30° N. This is due to the fact that atmospheric fronts are observed only in the extratropical zone and, in the Southern Hemisphere, the network of aerological stations is too sparse for our purpose, i.e., for the determination of quantitative

[4] Forecasts can have a small systematic error: for example, prognostic fields averaged over a month can differ from actual mean fields averaged over the same period [15].

[5] At present, it is the fields of deviations of data from the forecast for the term of analysis that are interpolated at the operational OA HMCs RF. In this case, the CFs for these deviations are used [4, 5].

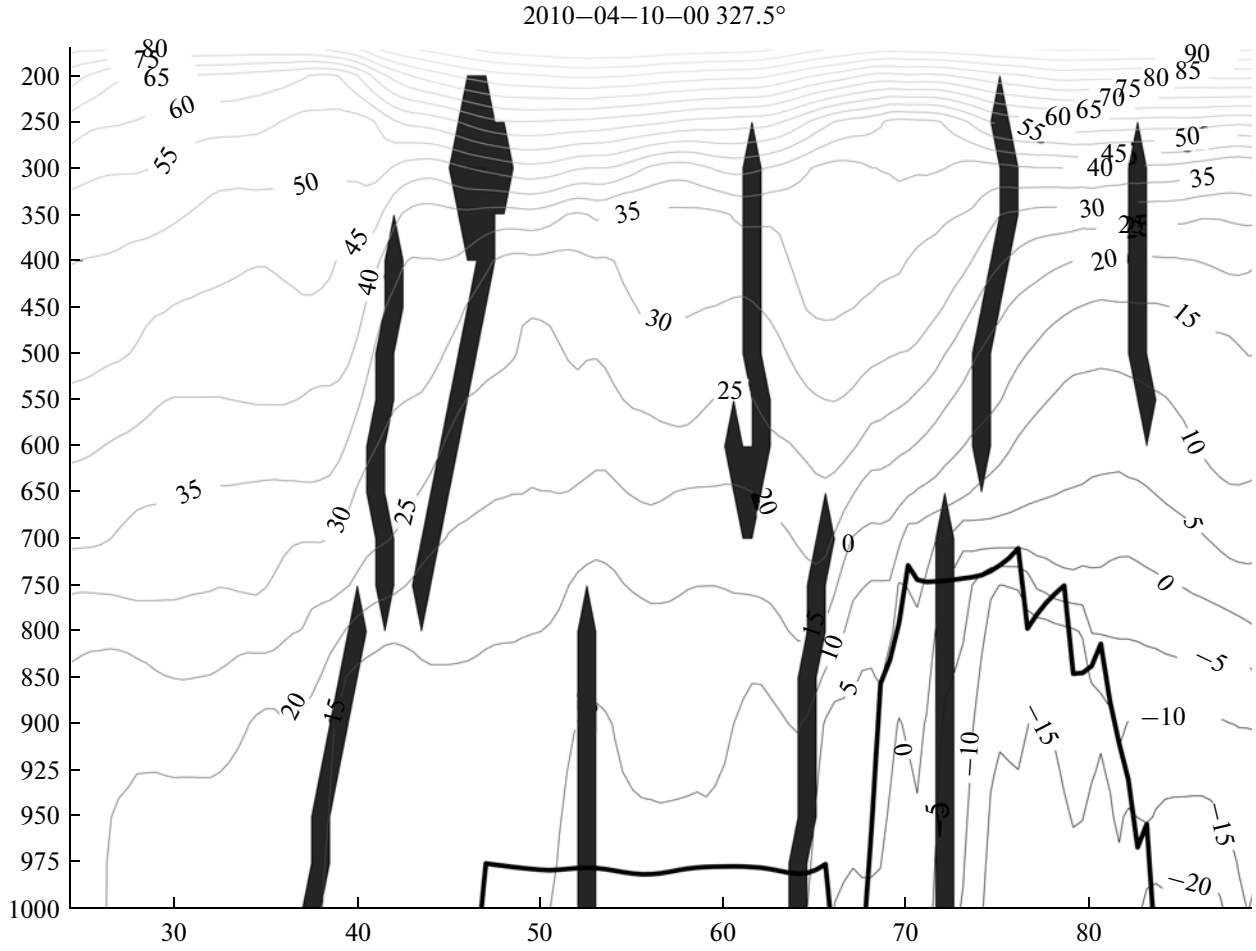

Fig. 5. Section along the meridian 32.5° W of the front calculated with the use of the optimal criterion (see Section 4) from the OA NCEP data for 00:00, December 24, 2009. Degrees of the northern latitude and the pressure (hPa) are plotted along the horizontal and vertical, respectively. The horizontal pattern can be seen in Fig. 4.

parameters of the algorithm for the diagnostics of atmospheric fronts.

We have chosen this limit for R because, first, at larger distances, absolute values of all CFs do not exceed 0.1 [12] and, second, in OA tasks, no such distances are usually used. If other distances that are close to R (within 2000–4000 km) are used in the experiments described below, all of the basic results change only slightly.

Inside each group, pairs of stations are divided into two subgroups: the first subgroup includes stations between which the front passes; the second subgroup includes the remaining stations (of course, this division into subgroups changes from one day to another and from one level to another). Calculating the correlations of values of meteorological fields for each group separately, we obtain two two-dimensional CFs for the case A, when pairs of points are separated by the frontal zone, and for the case B, when pairs of points are not separated by the frontal zone. The relation between the frequencies of cases A and B is shown in Fig. 6.

As a result, we obtain two stepped (with the step Δr) matrix-valued CFs: $S_{ij}(r)$ corresponding to case A and $U_{ij}(r)$ corresponding to case B. Here and below, $i, j = 1, 2, 3, 4$; the first, second, third, and fourth components correspond to temperature, geopotential, longitudinal wind component, and transverse wind component, respectively.

3.4. Smoothing of Correlation Functions

To choose the optimal criterion of the frontal zone, it is necessary to be capable of estimating the distinction between the air masses on different sides of the front at a given criterion and, consequently, to be able to estimate the distinctions between the CFs for cases A and B.

The simplest ways of estimating these distinctions are as follows:

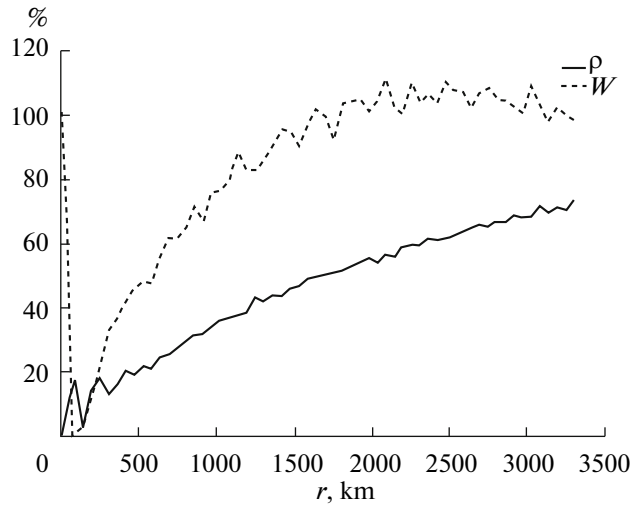

Fig. 6. Statistics of the separation of meteorological stations by the front. The solid line (ρ) is the fraction of pairs of stations separated by the front among all pairs of stations, depending on the distance r (km). The dashed line (W) is the ratio of the pairs of stations located at distances $(r-25, r+25)$ to the total number of stations. Therefore, the numbers of stations related to cases A and B are $w = MW\rho$ and $w = MW(1-\rho)$, respectively (here, M is the number of stations). Only the pairs of stations located to the north from 30° N were considered).

(1) The norm of the difference between the CFs $S_{ij}(r)$ and $U_{ij}(r)$ in the metrics $L^2[\mathbb{R}_+]$.

(2) As (1), but taking into account the number of measurements at the pairs of stations located in a given range of distances (see plot W in Fig. 6).

(3) As (1), but normalized to the sum of the L^2-norm: $\frac{\|S_{ij}-U_{ij}\|}{\|S_{ij}\|+\|U_{ij}\|}$.

However, since the sample is not sufficiently large, we can directly use none of these variants with the CFs estimated in the preceding subsection, because they strongly oscillate, and the estimates obtained are unreliable. For obtaining high-quality estimates, preliminary smoothing is necessary.[6]

According to the Bochner theorem [14, 16], positively defined CFs of a scalar isotropic homogeneous field expand into the Fourier–Bessel integral:

$$K(r) = a_0\delta(r) + \int_{k=0}^{\infty} a(k)\mathbf{J}_0(kr)k\,dk,$$

where $a_0 + \int_{k=0}^{\infty} a(k)k\,dk = 1$, $a_0 \geqslant 0$, and $a(k) \geqslant 0$; $\mathbf{J}_0$ is the zero Bessel function and δ is the delta function.

If CFs for several scalar fields (for example, the fields of temperature and geopotential) are estimated together, the coefficients a_0 and $a(k)$ in this theorem are replaced by the symmetrical positively defined matrices A_0 and $A(k)$. In the experiments described below, the four-component random field consists of these scalar fields and the longitudinal and transverse wind components. The auto- and cross-correlations for the wind components must be expanded in terms of $-J_0''(kr)$, and their cross-correlations with scalar fields must be expanded in terms of $J_0'(kr)$ (here, ' (prime) means the derivative with respect to r). For more detail, see [7, 12, 14, 16].

Let us introduce the prenorm[7] in the CF space with weights proportional to the number of pairs of measurements in the power 2/3, which fell into a given distance interval:

$$\|S(r)\|_{\mathrm{CF}} = \frac{1}{\sum_{s=0}^{M} w(s)^{2/3}} \sum_{s=0}^{M} w(s)^{2/3} \sum_{i,j=1}^{4} S_{ij}^2(s\Delta r), \qquad (7)$$

where $M = R/\Delta r$, and $w(s)$ is the number of pairs of measurements for the case under consideration, which are spaced from each other by no more than $(s-1)\Delta r$ but less than $s\Delta r$.

Let us find the positively defined CF, closest in the sense of prenorm (7), to the function $S_{ij}(r)$ obtained through a direct estimation. This is necessary because there are many gaps in measurement data, and no positive definiteness is guaranteed for estimates of CFs of the $S_{ij}(r)$ type. We will analogously treat $U_{ij}(r)$.

Changing matrices A^n, we approximate, using the least squares method, the matrix-valued correlation function $S(r)$ by the functions having the form

$$K_{A_0,\ldots,A_N}(r) = A^0\delta(r) + \sum_{n=1}^{N} \mathscr{J}^n(A^n, k_n r), \qquad (8)$$

where $k_n \geqslant 0$ are positive scale multipliers and $\mathscr{J}^n$ is the symmetric matrix-valued function:

$$\mathscr{J}^n(A^n, y) = \begin{Vmatrix} \delta_n a_{11}^n \mathbf{J}_0(y) & \delta_n a_{12}^n \mathbf{J}_0(y) & \vartheta_n a_{13}^n \mathbf{J}_0'(y) & \vartheta_n a_{14}^n \mathbf{J}_0'(y) \\ \delta_n a_{21}^n \mathbf{J}_0(y) & \delta_n a_{22}^n \mathbf{J}_0(y) & \vartheta_n a_{23}^n \mathbf{J}_0'(y) & \vartheta_n a_{24}^n \mathbf{J}_0'(y) \\ \vartheta_n a_{31}^n \mathbf{J}_0'(y) & \vartheta_n a_{32}^n \mathbf{J}_0'(y) & -\varepsilon_n a_{33}^n \mathbf{J}_0''(y) & -\varepsilon_n a_{34}^n \mathbf{J}_0''(y) \\ \vartheta_n a_{41}^n \mathbf{J}_0'(y) & \vartheta_n a_{42}^n \mathbf{J}_0'(y) & -\varepsilon_n a_{43}^n \mathbf{J}_0''(y) & -\varepsilon_n a_{44}^n \mathbf{J}_0''(y) \end{Vmatrix},$$

where δ_n, ε_n, and $\vartheta_n = \sqrt{\delta_n\varepsilon_n}$ are the normalizing coefficients, which were chosen in the following way:

[6] The projection of CFs on a finite-dimensional cone in the space of positively defined CFs: i.e., we perform the regularization of the CF estimate.

[7] This and other prenorms close to it ensure a good approximation of a CF if the number of measurements is different for different values of r.

Table 2. Characteristic values of errors $e(k_1, \ldots, k_N)$ of the approximation CF $S_{ij}(r)$ of the positively defined CF of kind (8) depending on N

N	2	3	4	5	6	7	8	9
$e(k_1,\ldots,k_N)$	0.00074	0.000636	0.00054	0.000503	0.000415	0.000378	0.000322	0.000273

$\delta_n^{-1} = \left\|\mathcal{J}^n(A', k_n r)\right\|_{\mathrm{CF}}$, and $\varepsilon_n^{-1} = \left\|\mathcal{J}^n(A'', k_n r)\right\|_{\mathrm{CF}}$, where A' is the matrix with only one nonzero element $A'_{11} = 1$, and A'' is the matrix with the nonzero element $A''_{33} = 1$. Therefore, the CF is approximately expended in terms of N normalized Bessel functions. The experiments were conducted at $N = 2, \ldots, 10$.

Then, we replace the matrices $A^n = \left\|a_{ij}^n\right\|$ by the positively defined symmetric matrices $B^n = \left\|b_{ij}^n\right\|$ (the corresponding algorithm based on the perturbation theory of self-adjoint operators is described in [4, 5, 7, 12]) nearest to them.

Performing this replacement, we should take into account linear limitations: the matrices B^n must be such that unities stood along the diagonal in the matrix $K_{B^0,\ldots,B^N}(0)$, and the matrix B^0 must have the following form:

$$B^0 = \begin{Vmatrix} b_{11}^0 & b_{12}^0 & 0 & 0 \\ b_{12}^0 & b_{22}^0 & 0 & 0 \\ 0 & 0 & b_{33}^0 & 0 \\ 0 & 0 & 0 & b_{33}^0 \end{Vmatrix}.$$

Now, we explain the choice of the normalizations δ_n and ε_n in the function $\mathcal{J}^n(A, r)$. The norm $\left\|\mathbf{J}_0''(k_n r)\right\|_{\mathrm{CF}}$ has the order k_n^2, and at relatively small values of k_n (about 20) (here, r was measured in thousands of kilometers), in order to ensure the order $c = 1/1000$, sometimes we have to change matrix A (if it is not positively defined) too strongly (by a magnitude of no less than $\sim ck_n^2 = 0.4$), and the main hypothesis of the perturbation theory is not fulfilled. No such problem arises at the chosen normalizations of matrices.

The scale multipliers $k_1, \ldots, k_N$ in arguments of the Bessel function also must be optimized. To do this, after replacing the CF by approximation (8), we calculate the error of approximation in the sense of the premetrics produced by prenorm (7):

$$e(k_1,\ldots,k_N) = \sqrt{\left\|S(r) - K_{B^0,\ldots,B^N}(r)\right\|_{\mathrm{CF}}}.$$

For each level and separately for cases A and B, we first enumerated 400 pairs of characteristic values of k_1 (in the range 0.01–15) and k_2 (in the range 10–70). For these values we calculated the errors $e(k_1, k_2)$, and the pair with the minimal $e(k_1, k_2)$ was taken as a first approximation. Then $e(k_1, k_2)$ was minimized by the gradient descent method.

Now, we choose the first approximation $k_3 = 1.5k_2$ and minimize by the gradient descent method $e(k_1, k_2, k_3)$ and so on. Having performed $N = 2$ steps, we find the best approximation of our function by the function of kind (8).

The approximate dependence of the error of the approximation $e(k_1, \ldots, k_N)$ is shown in Table 2. Subsequently, we used the value $N = 5$, because no further increase of N substantially decreases the error.

If the fields are normalized to deviations from the monthly mean values (see Subsection 3.2) before the CF calculation, the diagonal values of the matrix A^0 will be interpreted as the mean variance of instruments (sondes), which were used for measuring meteorological field values. If the fields are normalized to deviations from prognostic values, the diagonal values of the matrix A^0 will be interpreted as the accuracy of the prognostic scheme.

3.5. Estimation of the Difference of Correlation Functions

Having performed the described operations with CFs in cases A and B, we obtain two matrix-valued correlation functions S_{ij} and U_{ij}. The difference between them is estimated by the formula

$$d_{ij} = \int_0^R \left|S_{ij} - U_{ij}\right|^2 r dr.$$

The total difference between the two CFs is estimated as the sum

$$d = \frac{\sum_{i,j=1}^{4} w_{ij} d_{ij}}{\sum_{i,j=1}^{4} w_{ij}}, \qquad (9)$$

Table 3. Optimal values of α and β, at which the maximal difference $d(\alpha, \beta)$ between the CFs $S_{ij}(r)$ and $U_{ij}(r)$ is attained depending on the level; the corresponding coefficients of renormalization $\mu_{\alpha\beta}$; and errors of the CF smoothing

Level, hPa	α	β	$1 - \alpha - \beta$	$\mu_{\alpha\beta}$	$d(\alpha, \beta)$	$e_5^S(\alpha,\beta)$	$e_5^U(\alpha,\beta)$
February							
300	0.682	0.0582	0.259	0.992	0.0733	0.00141	0.00176
400	0.726	0.0558	0.218	1.07	0.0963	0.00177	0.00407
500	0.753	0.0545	0.192	0.968	0.0796	0.0019	0.00596
700	0.785	0.0545	0.161	0.855	0.0634	0.00172	0.00178
850	0.799	0.056	0.145	0.823	0.0569	0.00139	0.00214
925	0.805	0.057	0.138	0.799	0.0595	0.00155	0.0025
1000	0.809	0.0583	0.132	0.76	0.0805	0.00573	0.0076
June							
300	0.727	0.0506	0.223	0.965	0.103	0.00189	0.00185
400	0.772	0.0437	0.184	1.09	0.107	0.0021	0.00156
500	0.8	0.0391	0.161	1.04	0.0973	0.00229	0.00168
700	0.833	0.0339	0.133	0.852	0.0633	0.00198	0.002
850	0.848	0.0325	0.12	0.769	0.0522	0.003	0.00185
925	0.854	0.0322	0.114	0.757	0.0557	0.0024	0.00206
1000	0.859	0.0323	0.109	0.765	0.0955	0.0117	0.0107

where $w_{ij} \geq 0$ are the weight coefficients. Here we used the following weights:

$$W = \begin{vmatrix} 2 & 1 & 1 & 1 \\ 1 & 2 & 1 & 1 \\ 1 & 1 & 2 & 1 \\ 1 & 1 & 1 & 2 \end{vmatrix}. \qquad (10)$$

The twos on the diagonal of the weight matrix W compensate the "inequality": the matrix d_{ij} is symmetric and, consequently, nondiagonal elements contribute twice to sum (9).

4. OPTIMAL COMBINATIONS OF FRONT PREDICTORS

In Section 1, we constructed various predictors of the atmospheric front. For any predictor field P, we can estimate the CFs $S_{ij}(r)$ and $U_{ij}(r)$. The difference between these functions shows how strongly air masses on both sides of the constructed frontal zones, and thereby the quality of construction of these zones, differ. Changing the field P, we try to achieve the largest difference d between the CFs $S_{ij}(r)$ and $U_{ij}(r)$. There is also a mechanism which allows us to affect the result of constructing frontal zones $C(\mathrm{P})$, i.e., the choice of the field P used in the algorithm described in Subsection 2.2.

The field P is the result of the action of a certain operator F on the main meteorological fields: temperature, geopotential, and wind. In Section 1, on the basis of each field, we constructed the following predictors for each baric level: the temperature gradient magnitude $G = |\nabla T|$, the largest eigenvalue of the Hesse matrix for the geopotential L, and the largest eigenvalue R of the matrix K for the wind. Now, we construct a complex predictor of the atmospheric front in the form of a certain function $F = F(G, R, L)$ monotonically increasing over all variables from the three given predictors.

The simplest monotonically increasing functions of three variables are linear with nonnegative coefficients. We will search for F in the form

$$F = F_{\alpha\beta} = \alpha G + \beta R + (1 - \alpha - \beta)L, \qquad (11)$$

where $0 \leq \alpha, \beta$ and $\alpha + \beta \leq 1$.

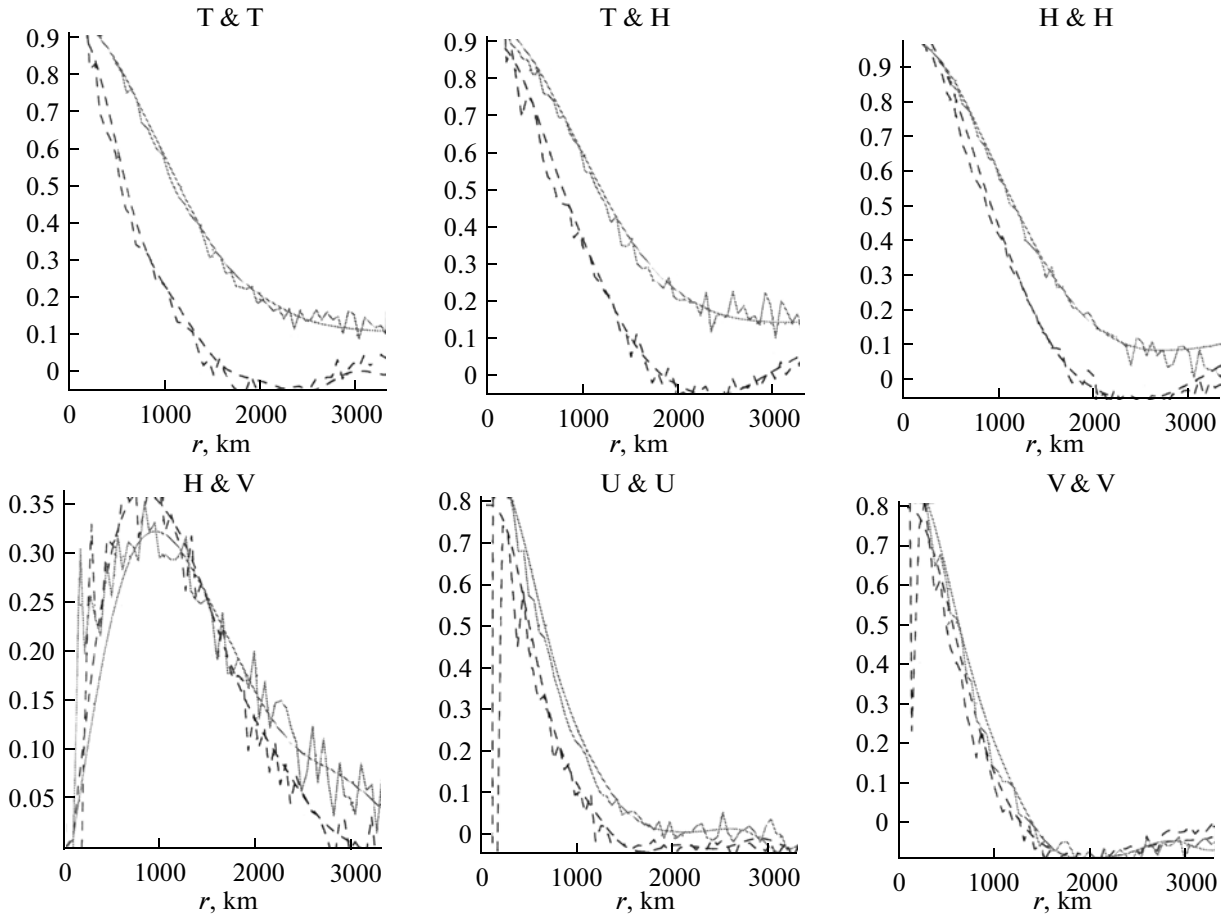

Fig. 7. Correlation functions at the level 400 hPa over April and the results of their smoothing. The dashed line is for case A, when points are separated by the frontal zone; the solid line is for case B, when points are not separated; u is the longitudinal wind component; and v is the transverse wind component.

4.1. Results of the Search for Optimal Predictors

Choosing the coefficients α and β from the set $\{0; 0.1; \ldots; 1\}$ so that $\alpha + \beta \le 1$ (in all, 66 pairs), we estimate the difference $d^{lm}(\alpha, \beta)$ between the CFs depending of the level l and the month m.

Since we must ensure a continuous dependence of the result on the time of the year and the level, we search for the optimal α and β in the form

$$\alpha = c_1 + c_2 \sin m + c_3 \cos m + c_4 l + c_5 \sin 2m + c_6 \cos 2m + c_7 l \sin m + c_8 l \cos m + c_9 l^2 + c_{10} l^3,$$

$$\beta = c_{11} + c_{12} \sin m + c_{13} \cos m + c_{14} l + c_{15} \sin 2m + c_{16} \cos 2m + c_{17} l \sin m + c_{18} l \cos m + c_{19} l^2 + c_{20} l^3,$$

where $m = \pi[M + (D - 15)/30 + (T + Z)/24/30]/6$; here, M is the number of the month, D is the number of the day, T is the time of the day, Z is the term of forecast (0 in the OA case), and

$$l = \frac{\ln p - \ln 1000}{\ln 300 - \ln 1000}.$$

From the values of $d^{lm}(\alpha, \beta)$, we construct for each level and month its own spline $d_s^{lm}(\alpha, \beta)$, whereupon we maximize the function

$$D(c_1, \ldots, c_{20}) = \frac{\sum_{m=1}^{12} \sum_{l=0}^{1} d_s^{lm}(\alpha, \beta) \sum_{r=0}^{3000} (w_U(\alpha, \beta) w_S(\alpha, \beta))^{1/3}}{\sum_{m=1}^{12} \sum_{l=0}^{1} \sum_{r=0}^{3000} (w_U(\alpha, \beta) w_S(\alpha, \beta))^{1/3}}$$

by the gradient descent method. The pairs of optimal α and β found for $m = 2$ and $m = 7$, together with the coefficients $\mu_{\alpha\beta}$ are presented in Table 3.[8]

[8] The coefficients of renormalization $\mu_{\alpha\beta}$ ensure the same mean areas of frontal zones at different α and β, which yields a correct comparison of different predictors.

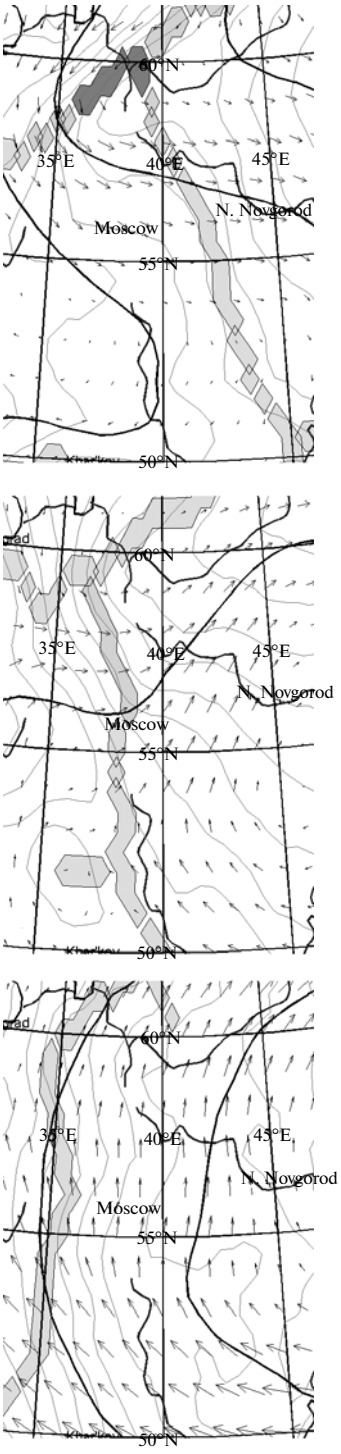

Fig. 8. Maps showing the frontal zones in the area of Moscow constructed with the use of the optimal criterion at the levels (from top to bottom) 500, 700, and 950 hPa. The contours of temperature (thin lines) and geopotential (thick lines) are drawn at intervals of 1° and 20 m, respectively; the wind field is presented on the 1° grid. Large rivers are also shown.

4.2. Results of an Estimation of Correlation Functions

The smoothed CFs for different fields at the level 400 hPa in April are presented in Fig. 7. In order to divide stations into cases A and B, we used the optimal criterion for each baric level determined in Subsection 4.1. This criterion was calculated on the basis of the OA archive on a grid with a step of 0.5° from November 2009 through December 2010 (in all, 336 terms).

Table 3 shows the results of a search for optimal front predictors. The values of $d(\alpha, \beta)$ show that, in February, the frontal activity maximum falls on the levels 400–500 hPa and, in July, it rises to the levels 300–400 hPa. This phenomenon justifies the choice of the level 400 hPa as the basic level for the vertical correlation of frontal zones (see Subsection 2.3).

5. EXAMPLES OF THE CONSTRUCTION OF FRONTAL ZONES

Let us consider in detail the meteorological fields for two days: December 7, 2009, and April 17, 2010. These two dates are remarkable in regards to the errors in the short-term forecasts of precipitation over Moscow maximal over the 2009–2010 winter period. In these cases, it was difficult for synoptic meteorologists to explain the forecast errors even at antedate. In the first case, the amount of precipitation forecast for Moscow was an order of magnitude smaller than the actual amount. In the second case, on the contrary, a substantial amount of precipitation during the atmospheric front passage was forecast; however, there was no precipitation at all. For our calculations, the OA NCEP data on the 0.5° grid were used.

The maps of frontal zones in the Moscow area on December 7, 2009, are shown in Fig. 8. Temperature contours are drawn at intervals of 1°C (thin lines), and geopotential contours are drawn at intervals of 20 m (thick lines). The wind field is plotted on the latitude–longitude grid with a step of 1°. Frontal zones are colored. It is seen (not only from these maps but from maps at all levels) that the atmospheric front actually passed and was located over Moscow with an eastward slope. The front was over Moscow at 00:00 at a height of about 700 hPa.

The maps of frontal zones in the Moscow area on April 17, 2010, are shown in Fig. 9. It is seen (not only from these maps but from maps at all levels) that no atmospheric front was detected over Moscow.

6. CONCLUSIONS

(1) Predictors of frontal zones ensuring a more exact description of frontal zones than the traditionally used vertical component of the wind velocity vortex and the horizontal Laplace operator from the geopotential (pressure at sea level) are proposed. The following parameters are used for a description of frontal

zones: the largest eigenvalues of the matrices consisting of first horizontal derivatives of the horizontal wind and second horizontal derivatives (Hesse matrices) of the geopotential (pressure at sea level), respectively.

(2) For calculations from data on a regular discrete two-dimensional grid, the exact methods based on a special discrete Fourier transform (in the case of a sphere) and compact schemes of the high-order (no lower than the fourth-order) approximation (in the case of a plane) are used instead of the traditional second-order methods.

(3) Heuristic methods for drawing atmospheric front lines along the ridges of predictor fields have been developed.

(4) Estimates of correlation functions (CFs) are obtained for clusters in a set of pairs of points: two points separated by the atmospheric front (belonging to different air masses) and not separated (belonging to the same air mass), respectively. Correlation functions were calculated for measurement data from aerological data normalized to their monthly mean values. The archive of observations accumulated by the authors and the OA NCEP data on the grid 0.5° × 0.5° over 336 days were used. The experiments were performed for the territory located to the north from 30° N. The distinctions between the CFs for two clusters can be taken into account in the assimilation of (OA) observational data for decreasing the error of the interpolation of observational data into grid points of a prognostic model.

(5) Methods of combining several (three) predictor fields are proposed, and the optimal weights for the initial predictors are selected experimentally for each baric level. The weights were optimized in accordance with the following criterion of quality: the maximal distinction between the CFs $S_{ij}(r)$ and $U_{ij}(r)$, i.e., between the CFs for the two clusters.

(6) The optimal coefficients for the predictors are calculated for each month and level. These coefficients are used for constructing the frontal zones correlated along the vertical at each level. In this case the frontal surfaces can contain holes, and these surfaces do not always extend from the earth's surface to the tropopause. Therefore, the graphic presentation of the results is nontrivial.

(7) The software developed for diagnosing the geometry of atmospheric fronts was also applied for diagnosing the prognostic fields of temperature, wind, and geopotential according to the NCEP model with the spatial resolution 0.5° × 0.5° and with forecast terms of 12, 24, and 36 h. At such forecast terms, the influence of errors in the prediction of fronts is comparatively weak. The topology of fronts is, on the whole, retained (about 4–6%, 6–9%, and 7–10% in the forecasts for 12, 24, and 36 h, respectively, of the total front lengths are not confirmed in the analysis, and the same amounts appear in the analysis); the mean front shift in passing from the predicted fields to

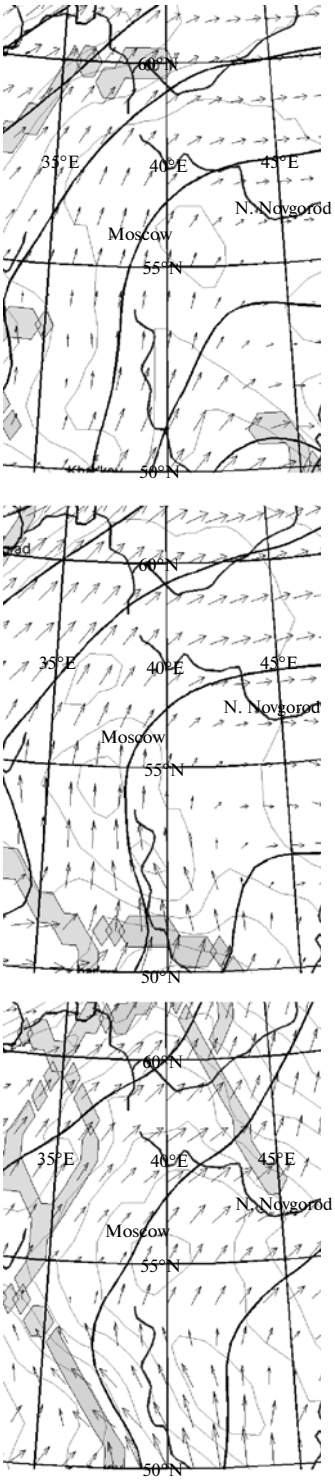

Fig. 9. Maps showing the frontal zones in the area of Moscow constructed for April 17, 2010, with the use of the optimal criterion at the levels (from top to bottom) 500, 700, and 950 hPa.

the OA fields for each term of forecast is about 60–70 km (regardless of the forecast term).

(8) It would be expected that the improvement of the OA spatial resolution and prognostic models and a higher accuracy of predictions of meteorological fields will also improve the quality of diagnosing the geometry of atmospheric fronts.

ACKNOWLEDGMENTS

We are grateful to M.G. Naitshuler and B.E. Peskov for useful discussions of the synoptic interpretation of our results, as well as to A.N. Bagrov and A.Yu. Nedachina for assistance in work with data bases of the Hydrometeorological Centre of Russia. This work was supported in part by the GU-HSE grant (TZ-47, 2009).

REFERENCES

1. L. D. Landau and E. M. Lifshits, *Hydrodynamics* (Nauka, Moscow, 1986).
2. N. E. Kochin, *Collection of Works*, Vol. 1 (USSR Akad. Sci., Moscow, 1949).
3. M. Geb, "New Aspects and Interpretations of the Concept of Air Masses and Fronts (Neue Aspekte und Interpretationen zum Luftmassen- und Frontenkonzept)," Meteorologische Abhandlungen, Freie Universität Berlin, **109** (2), (1971)
4. V. A. Gordin, *Mathematical Problems in Hydrodynamical Weather Forecasting. Computational Aspects* (Gidrometeoizdat, Leningrad, 1987) [in Russian].
5. V. A. Gordin, *Mathematical Problems and Methods in Hydrodynamical Weather Forecasting* (Gordon and Breach, Amsterdam, 2000).
6. J. Neissen, V. Görsdorf, and H. Steinhagen, *Instruments and Observing Methods* (WMO, Geneva, 1994), No. 57.
7. V. A. Gordin, *How It Should Be Computed? Meteorological Data Assimilation* (MCCME, Moscow, 2005) [in Russian].
8. V. A. Gordin and A. V. Khalyavin, "Projection Methods for Meteorological Data Noise Suppression before Derivative Computation," Meteorol. Gidrol., No. 10, 55–65 (2007).
9. V. A. Gordin, *Mathematical Problems in Hydrodynamical Weather Forecasting. Analytical Aspects* (Gidrometeoizdat, Leningrad, 1987) [in Russian].
10. V. A. Gordin, *Mathematics, Computer, Weather Forecast, and Other Scenarios of Mathematical Physics* (Fizmatlit, Moscow, 2010) [in Russian].
11. F. Huber-Pock and Ch. Kress, "An Operational Model of Objective Frontal Analysis Based on ECMWF Products," Meteorol. Atmos. Phys. **40** (4), 170–180 (1989).
12. O. A. Aldukhov and V. A. Gordin, "Three-Dimensional Correlation Functions of Basic Upper-Air Parameters," Izv., Atmos. Ocean. Phys. **37** (1), 1–20 (2001).
13. O. A. Aldukhov and V. A. Gordin, "Estimation of Anisotropy of Correlation Functions of Meteorological Fields from Global Upper-Air Observations," Izv., Atmos. Ocean. Phys. **41** (3), 361–370 (2005).
14. A. S. Monin and A. M. Yaglom, *Statistical Hydromechanics*, Vol. 1 (Gidrometeoizdat, Leningrad, 1992); Vol. 2 (Nauka, Moscow, 1996).
15. O. A. Aldukhov, A. N. Bagrov, and V. A. Gordin, "Statistical Characteristics of Prognostic Meteorological Field and Their Usage for Objective Analysis," Meteorol. Gidrol., No. 10, 18–33 (2002).
16. I. M. Gel'fand and N. Ya. Vilenkin, *Some Applications of Harmonic Analysis. The Framed Hilbert Spaces* (Fizmatlit, Moscow, 1961) [in Russian].